Citation information: DOI 10.1109/TIE.2018.2835387, IEEE

Modeling of HVDC Tie-Links and Their Utilization in AGC/LFC Operations of Multi-Area Power Systems

Nikhil Pathak, *Student Member, IEEE*, Ashu Verma, *Senior Member, IEEE,* T.S. Bhatti and Ibraheem Nasiruddin

***Abstract*— This paper presents the accurate modeling of HVDC links for the dynamic studies of automatic generation control/load frequency control (AGC/LFC) of multi-area interconnected power system. In earlier AGC studies, HVDC links were simply modeled by using the first-order transfer function with system time constant T_{dc}. It was argued that T_{dc} is the time required by HVDC links to establish DC current after following a load disturbance in power system. However, no mathematical or analytical justification was provided in support to the existing transfer function model of HVDC links. This paper presents the accurate modeling of HVDC links for AGC studies. The comparative analysis has also been performed to demonstrate error being accrued due to the use of conventional model of HVDC links. Furthermore, this paper also implements the inertia emulation based control (INEC) strategy in AGC which allows to harness the stored energy from the capacitance of HVDC links for AGC operations.**

***Index Terms*— Automatic generation control, AC−DC interconnections and discrete supplementary controllers.**

I. Nomenclature

i & j	Index referred to areas (i & $j = 1, 2, 3, \ldots$)
Δf & ΔP_{tie}	Frequency and tie-line power deviations
ΔP_g	Change in generator power output
P_r	Rated area capacity
B	Frequency bias factor
R	Speed regulation parameter
T_p & K_p	Power system time constant and gain constant
T_{SC}	Steam chest time constant
T_{RH} & K_{RH}	Reheater time constant and gain constant
T_{ij}	Synchronizing coefficient of tie-line
a_{ij}	Area capacity ratio ($-P_{ri}/P_{rj}$)

Manuscript received August 09, 2017; revised November 13, 2017, January 05, 2018 and February 17, 2018; accepted March 26, 2018.
(Corresponding author: Nikhil Pathak)

N. Pathak, A. Verma and T.S. Bhatti are with the Centre for Energy Studies, Indian Institute of Technology Delhi, New Delhi, India (e-mail: 2013niks@gmail.com; averma@ces.iitd.ac.in; tsb@ces.iitd.ac.in) .

I. Nasiruddin is with the Department of Electrical Engineering, College of Engineering, Qassim University, Buraidah 51452, Saudi Arabia, on leave from Jamia Millia Islamia University, New Delhi, India-110025. (e-mail: ibraheem_2k@yahoo.com)

II. Introduction

THE power system frequency is maintained to its nominal value by nullifying the power mismatch between active power generation and load demand using AGC. Numerous studies have been conducted so far upon multi-area interconnected thermal power systems considering non-reheat as well as reheat turbines [1−4]. The power system nonlinearities, such as, generation rate constraints (GRCs), governor dead-band effects were also considered [5]. The various meta-heuristic algorithms, such as, genetic, particle swarm optimization, bacterial foraging and harmonic search etc., were also developed for the optimization of supplementary controller gains [6−8]. The studies were further carried out for different loading conditions of power plants. It was discovered that power system model parameters, namely, turbine time constants (T_t), power system time and gain constants (T_p & K_p), frequency bias factor (B) also varies along with power system loading conditions and significantly affects the system dynamics [9]. The studies were further extended to discrete supplementary control of AGC system. The sampling period of 2s was selected for discrete AGC controllers [10].

Nowadays, drastic increase of load demand in power system areas raised the necessity of increasing inter-area power transfer capabilities. The HVDC links are being added in parallel to existing AC links to increase the power transfer capacity of tie-links. Recently, lot of researchers studied the effect of HVDC links on the dynamic of performance of AGC system [11−17]. In these studies, HVDC links were simply represented by first-order transfer function with time constant and gain constant T_{dc} & K_{dc}, respectively. It was stated that T_{dc} is the time taken by HVDC system to establish DC current after having a small load perturbation. Furthermore, the value of K_{dc} was selected so that the system exhibits improved dynamic performance. Furthermore, HVDC links were also studied in transient stability studies of power systems, such as, line faults analysis, large power system load disturbances etc. The INEC strategy was developed to utilize the capacitive stored energy of HVDC links during sudden load changes and line faults. The non-linear models of INEC were developed for these transient stability studies. In [18], INEC strategy was implemented upon a small system comprising of offshore wind farm at one end of HVDC link and a single synchronous generator on the other end. The study was further extended in which the INEC strategy was combined with the control strategy utilizing inertial response of wind turbines in order to

Citation information: DOI 10.1109/TIE.2018.2835387, IEEE

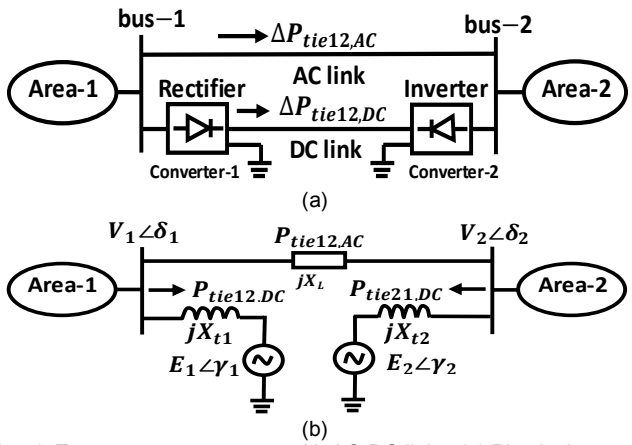

Fig. 1. Two area power system with AC-DC links: (a) Physical system and (b) Equivalent model.

support primary frequency control [19]. The INEC strategy was also implemented upon HVDC system comprising of various industrial loads, such as, induction motor, resistive load, diode rectifier load etc [20]. In this study, vector control or d-q control was utilized to control the voltage level of VSC-HVDC links. The same control strategy was also implemented upon multi-terminal HVDC systems [21, 22]. The frequency support capability HVDC system based on INEC strategy was also studied [23−25]. Based on literature survey, following research gaps have been found and addressed in this paper:

1) No mathematical or analytical procedure was provided in support to the existing first-order transfer function model of HVDC links. Furthermore, no guidelines were given in order to calculate model parameter values of HVDC links. This paper fulfills the aforementioned research gaps and presents the modeling of HVDC links in AGC studies. For the first time, transfer function model of HVDC link has been derived mathematically with proper physical as well as analytical justifications. The comparative analysis has also been carried out with existing model of HVDC links to demonstrate the error being accrued in AGC studies due to the use of conventional model of HVDC links.

2) The INEC strategy has been widely used in various transient stability studies of power systems to utilize the stored energy of HVDC links as well as other energy storage devices. This paper implements the same INEC strategy in AGC for frequency support applications. The linearized model of INEC strategy has been developed to utilize the stored energy of HVDC links in AGC operations. Alongside physical as well as analytical justifications, INEC control strategy has been successfully implemented upon two-area reheat thermal power systems interconnected via parallel AC−DC links.

III. Modeling of HVDC Links for AGC System

This section presents the accurate modeling of HVDC links in AGC system. The conventional model of HVDC link has also been discussed. These studies are as follows:

A. Conventional Model of HVDC Links:

The two area power system has been shown in Fig. 1(a). The DC link consists of rectifier and inverter which are controlled by adjusting their respective firing angles. The tie-line power deviations through AC and DC links have been denoted as $\Delta P_{tie,AC}$ and $\Delta P_{tie,DC}$, respectively. According to existing models, DC link is represented by the following first order transfer function given as follows [11−17]:

$$\Delta P_{tie,DC} = K_{dc}/(1 + T_{dc}s) \tag{1}$$

Where, T_{dc} represents the time required to establish DC current in HVDC link after following a small load disturbance in the power system area and K_{dc} represents the gain constant of HVDC link. The values of T_{dc} and K_{dc} was selected as 0.2s and 1.0, respectively. The literature review shows that the conventional transfer function model of HVDC link is based on simplified assumptions and never been derived analytically. No analytical or mathematical procedure was provided to estimate the values of T_{dc} and K_{dc}. Moreover, the conventional model of HVDC link also fails to relate any physical parameters such as rated capacity, voltage level, impedances of converters, loading of HVDC links etc. All these drawbacks have been addressed in the proposed accurate model of HVDC links.

B. Proposed Model of HVDC Links:

In Fig. 1(a), observing the AC-DC link from buses−1 & 2, HVDC link can be seen as a synchronous machine without inertia which can produce or consume the active and reactive powers independently. The aforementioned interpretation of HVDC link leads to the modeling of HVDC system as two controllable voltage sources connected in series with the phase reactors impedances [26, 27], as shown in Fig. 1(b).

The controllable voltage sources with their respective phase angles are denoted as: E_1, E_2, γ_1 and γ_2. The impedances of rectifier and inverter side phase reactors are denoted as X_{t1} and X_{t2}, respectively. The power injected from bus−1 & 2 into HVDC link are denoted by $P_{tie\,12,DC}$ and $P_{tie\,21,DC}$.

The power injected from bus−1 into HVDC link has been obtained using the following expression:

$$P_{tie\,12,DC} = (V_1E_1/X_{t1})\sin(\delta_1 - \gamma_1) \tag{2}$$

Upon linearizing Eqn. (2), following expression is obtained:

$$\Delta P_{tie\,12,DC} = (V_1E_1/X_{t1})\cos(\delta_1^0 - \gamma_1^0)\,(\Delta\delta_1 - \Delta\gamma_1) \tag{3}$$

Or,

$$\Delta P_{tie\,12,DC} = T_{12,DC}(\Delta\delta_1 - \Delta\gamma_1) \tag{4}$$

Where: $T_{12,DC} = (V_1E_1/X_{t1})\cos(\delta_1^0 - \gamma_1^0)$ represents the synchronization coefficient of rectifier side phase reactor.

Similarly, the power injected from bus−2 into HVDC link has been obtained given as follows:

$$\Delta P_{tie\,21,DC} = T_{21,DC}(\Delta\delta_2 - \Delta\gamma_2) \tag{5}$$

Where: $T_{21,DC} = (V_2E_2/X_{t2})\cos(\delta_2^0 - \gamma_2^0)$ represents the synchronization coefficient of inverter side phase reactor. The Eqns. (4) & (5) represents the expression of tie-line power deviations of the same HVDC link. These equations can simply be equated with a negative sign. The transmission line and power device losses are almost remains constant during load perturbations. Hence, deviations in the line losses will be negligible and therefore neglected. Based on the aforementioned assumptions, following equation has been obtained:

$$\Delta P_{tie\,12,DC} = -\Delta P_{tie\,21,DC} \tag{6}$$

Putting the values of $\Delta P_{tie\,12,DC}$ and $\Delta P_{tie\,21,DC}$ from Eqns. (4) and (5) into Eqn. (6), we get:

Citation information: DOI 10.1109/TIE.2018.2835387, IEEE

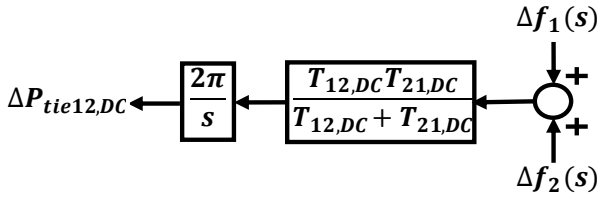

Fig. 2. Proposed accurate model of HVDC tie-links.

$$T_{12,DC}(\Delta\delta_1 - \Delta\gamma_1) = -T_{21,DC}(\Delta\delta_2 - \Delta\gamma_2) \quad (7)$$

To transmit the tie-line power from one area to the other via HVDC links, it is essential that both side converters are well synchronized. In other words, it can be stated that the change in rectifier's phase angle ($\Delta\gamma_1$) must be equal to the change in inverter's phase angle ($\Delta\gamma_2$) in order to transfer a specified amount of power between interconnected areas. Hence, it can be written as: $\Delta\gamma_1 = \Delta\gamma_2 = \Delta\gamma$. Putting these values in Eqn. (7), the following expression is obtained:

$$\Delta\gamma = \left[\Delta\delta_1 + \left(\frac{T_{21,DC}}{T_{12,DC}}\right)\Delta\delta_2\right] \Big/ \left[1 + \left(\frac{T_{21,DC}}{T_{12,DC}}\right)\right] \quad (8)$$

Putting back the value of $\Delta\gamma$ in Eqn. (4) and further solving the equation, we found:

$$\Delta P_{tie\,12,DC} = \left[T_{12,DC}T_{21,DC}/\left(T_{12,DC} + T_{21,DC}\right)\right](\Delta\delta_1 - \Delta\delta_2) \quad (9)$$

Or, $\Delta P_{tie\,12,DC} = 2\pi\left[T_{12,DC}T_{21,DC}/\left(T_{12,DC} + T_{21,DC}\right)\right]\int(\Delta f_1 - \Delta f2dt$ (10)

Taking the Laplace transform on both sides of Eqn. (10):

$$\Delta P_{tie\,12,DC}(s) = \left(\frac{T_{12,DC}T_{21,DC}}{T_{12,DC} + T_{21,DC}}\right)\frac{2\pi}{s}(\Delta f_1(s) - \Delta f_2(s)) \quad (11)$$

Or, $\Delta P_{tie\,12,DC}(s) = \left(2\pi T_{eqv}/s\right)(\Delta f_1(s) - \Delta f_2(s))$ (12)

Where: $T_{eqv} = T_{12,DC}T_{21,DC}/\left(T_{12,DC} + T_{21,DC}\right)$ represents the equivalent synchronization coefficient of HVDC link. The Eqn. (12) establishes the relationship between frequency deviations of interconnecting areas and tie-line power deviations of HVDC link. The corresponding transfer function model of HVDC link has been shown in Fig. 2.

For the comparative analysis between the synchronization coefficients of HVDC and AC links, Eqns. (2)−(12) have been solved further in Appendix I. Eqn. (52) of Appendix I shows that the synchronization coefficient of HVDC link is just half to that of AC link provided both tie-links exhibits same power transfer capacities and have been loaded equally.

C. Physical as well as Analytical Interpretation of Proposed Model of HVDC Links:

It has been observed from the proposed model that the HVDC links exhibits their own synchronization coefficient similar to the AC links. Hence, it can be stated that the exchange of power through HVDC links relies upon the synchronization coefficients of rectifier as well as inverter side phase reactors denoted as: $T_{12,DC}$ and $T_{21,DC}$, respectively. The mathematical expression of these synchronization coefficients reveals that $T_{12,DC}$ and $T_{21,DC}$ are dependent upon the physical parameters of HVDC links, such as, voltage level, bus angle difference and impedances of both side inverters employed to regulate the active power flow of HVDC links. Based on these physical parameters values of HVDC links, the value of HVDC synchronization coefficient are obtained. Furthermore, it has also been proven analytically that the synchronization coefficient of HVDC link is just half to that of AC link synchronization coefficient for equal power transfer capabilities and loadings of both tie-links.

Here, it is important to note that in previous AGC studies, first-order transfer function model was used in simulation studies irrespective to the topologies (LCC/VSC) used to operate HVDC links. Surprisingly, no information was provided regarding the topology for which first-order model was developed. However, in this paper, proposed model of HVDC link has been developed for VSC topology. The fundamental difference between these two topologies is that the reactive power cannot be controlled independent of the active power in case of LCC topology. However, in case of VSC topology, active as well as reactive powers both can be controlled independently. It is because of the fact that the control system of LCC topology has only the capability of 'turn-on' operation of semiconductor devices and relies on external AC system for 'turn-off' operation. Hence, the control system of LCC topology has only one-degree of freedom. However, in case of VSC topology, control system exhibits both capabilities of turning 'on' and 'off' operations of semiconductor devices and has the two-degree of freedom. This two degree of freedom of control system gives the capability to VSC topology to control the active and reactive powers independently. Based on the aforementioned fact, in the proposed model, active and reactive powers have been decoupled and the equivalent circuit has been developed for VSC topology of HVDC links.

D. Synchronization Coefficient Calculations:

The calculations of AC and HVDC link synchronization coefficients are given as follows:

1) AC link synchronization coefficients calculations

Max power transfer capability:

$$P_{max,AC} = V_1V_2/X_L = 200MW \quad (13)$$

Rated capacity of area-1: $P_{r1} = 2000MW$

Loading of AC link: $P_{tie\,12,AC} = 50\%$ or $100MW$

Bus angle difference required for 50% loading:

$$P_{tie\,12,AC} = P_{max,AC}\sin(\delta_1^0 - \delta_2^0) \quad (14)$$

Or, $$100 = 200\sin(\delta_1^0 - \delta_2^0) \quad (15)$$

$$\delta_1^0 - \delta_2^0 = 30° \quad (16)$$

AC link synchronization coefficient:

$$T_{12,AC} = \frac{P_{max,AC}}{P_r}\cos(\delta_1^0 - \delta_2^0) \quad (17)$$

$$T_{12,AC} = 0.0865 \quad (18)$$

2) DC link synchronization coefficient calculations

Max power transfer capability:

$$P_{max,DC} = V_1E_1/X_{t1} = V_2E_1/X_{t2} = 600MW \quad (19)$$

Rated capacity of area-1, 2: $P_{r1} = 2000MW$, $P_{r2} = 1000MW$

Loading of HVDC link: $P_{tie\,12,DC} = 50\%$ or $300MW$

Bus angle difference required between bus-1 and rectifier (converter-1) for 50% loading condition:

$$P_{tie\,12,DC} = P_{max,DC}\sin(\delta_1^0 - \gamma_1^0) \quad (20)$$

Or, $$300 = 600\sin(\delta_1^0 - \gamma_1^0) \quad (21)$$

Or, $$\delta_1^0 - \gamma_1^0 = 30° \quad (22)$$

Similarly, bus angle difference required between bus-2 and inverter (converter-2) for 50% loading condition has been obtained given as follows:

$$\delta_2^0 - \gamma_2^0 = 30° \quad (23)$$

Citation information: DOI 10.1109/TIE.2018.2835387, IEEE

TABLE I PHYSICAL DATA FOR VSC-HVDC LINK

Components	*Values*
VSC-HVDC capacity, S_{VSC}	600 MW
Rated DC voltage, V_{DC}	300 kV
DC capacitance, C_{DC}	0.148 mF
Number of capacitors, N	2 (Three level neutral-point clamped VSC)
Inertia constant, H_{VSC}	4s
Current Loading	50% or 300 MW
Synchronization coefficient T_{eqv}	$T_{12,DC}T_{21,DC}/(T_{12,DC}+T_{21,DC})$= 0.1732

TABLE II PHYSICAL DATA FOR AC LINK

Components	*Values*
AC-line max power transfer capacity, P_{max}	200 MW
Current Loading	50% or 100MW
Synchronization coefficient $T_{12,AC}$	0.0865

TABLE III SYNCHRONIZATION COEFFICIENTS OF HVDC LINK FOR DIFFERENT LOADING CONDITIONS

Tie-link loading	*Angle diff. of phase reactors* $(\delta_1^0-\gamma_1^0)=(\delta_2^0-\gamma_2^0)$	*Synchronization coefficient* (T_{eqv})
90%	64.15°	0.0867
50%	30.00°	0.1732
20%	11.53°	0.1954

Rectifier's synchronization coefficient:

$$T_{12,DC}=\frac{P_{max,DC}}{P_{r1}}\cos(\delta_1^0-\gamma_1^0)=\frac{600}{2000}\cos 30° \quad (24)$$

Or, $$T_{12,DC}=0.2598 \quad (25)$$

Inverter's synchronization coefficient:

$$T_{21,DC}=\frac{P_{max,DC}}{P_{r2}}\cos(\delta_2^0-\gamma_2^0)=\frac{600}{1000}\cos 30° \quad (26)$$

Or, $$T_{21,DC}=0.5196 \quad (27)$$

Hence, equivalent HVDC link synchronization coefficient can be calculated given as follows:

$$T_{eqv,DC}=\frac{T_{12,DC}T_{21,DC}}{T_{12,DC}+T_{21,DC}}=0.1732 \quad (28)$$

Here, the calculations of synchronization coefficients of AC and HVDC links have been shown only for 50% loading. The synchronization coefficients for other loading conditions can be calculated using the same procedure.

It has also been observed that similar to synchronization coefficients AC links, HVDC synchronization coefficients are also depends upon the loading of HVDC links. As the loading of HVDC links increases, the value of synchronization coefficient also increases. The physical data of AC as well as HVDC links with their respective synchronization coefficient values for different loading conditions have been shown in Tables I–III, respectively.

IV. INERTIA EMULATION CONTROL STRATEGY IN AGC

Typically, HVDC links can be considered as DC capacitors in which the electro-static energy is stored. This stored energy in HVDC link capacitors can be harnessed to provide the initial active power support in AGC operation. In the proposed control strategy, stored energy of HVDC link capacitors has been controlled in proportion to the grid frequency by regulating the HVDC link voltage. The control strategy emulates the synthetic inertia of HVDC links and has been termed as 'inertia emulation based control' (INEC) strategy. The complete control scheme of INEC strategy for two-area AGC system has been shown in Fig. 3. It has been observed that the frequency signals of both areas are transmitted to INEC strategy. Based on area frequency deviations, INEC strategy produces required voltage level of HVDC link in order to consume/release the stored energy of DC capacitance into electric power system network. The voltage control signal is sent to vector controllers to adjust the firing angles of both side converters. The mathematical modeling of INEC strategy for AGC operations is given as follows:

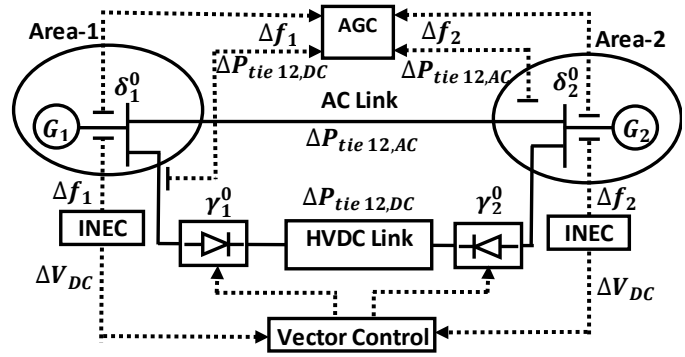

Fig. 3. Control scheme of INEC strategy for AGC operation.

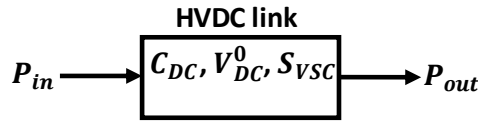

Fig. 4. HVDC Link Considered as DC Capacitor.

A. Proposed Model of INEC Strategy for the Utilization of Stored Energy of HVDC Links:

Generally, the electro-static energy stored in a capacitor is similar to mechanical (inertial) energy stored in a synchronous machine [18]. The typical angular motion equation of a synchronous machine is given as follows:

$$(2H/f^0)\frac{d}{dt}(\Delta f)=\Delta P_{mech}-\Delta P_{elect}=\Delta P_1\ p.u. \quad (29)$$

Where, H is inertia constant (*seconds*), f^0 is nominal frequency (*Hz*), ΔP_{mech} and ΔP_{elect} are the incremental changes in mechanical and electrical power outputs (*p.u.*).

The HVDC link having rated DC voltage V_{DC}^0, rated power capacity of VSC-inverters S_{VSC} and DC capacitance C_{DC} is shown in Fig. 4. The difference between input and output powers P_{in} and P_{out} of HVDC link results the fluctuations in system DC voltage. The capacitor dynamics in terms of DC voltage and power output can be written as follows:

$$NC_{DC}V_{DC}\frac{d}{dt}(V_{DC})=P_{in}-P_{out}=P_2\ MW \quad (30)$$

Where, N represents the number of capacitors in HVDC link. The Eqn. (30) shows that change in DC voltage also changes the stored energy of DC capacitors. This energy may be charged or discharged into the AC network depending upon the system need (during load disturbances) by controlling DC voltage level of HVDC links. Expressing Eqn. (30) in per unit by dividing it with the inverter's rated capacity S_{VSC}, we get:

$$(NC_{DC}/S_{VSC})V_{DC}\frac{d}{dt}(V_{DC})=P_2\ p.u. \quad (31)$$

Linearizing Eqn. (31) with respect to operating point V_{DC}^0:

$$(NC_{DC}V_{DC}^0/S_{VSC})\frac{d\Delta V_{DC}}{dt}=\Delta P_2\ p.u. \quad (32)$$

Further task is to allocate the exact value of inertia time constant H_{VSC} to HVDC link. Therefore, equating the equation of electrical machine angular motion, Eqn. (29) to the equation of capacitor's voltage dynamics, Eqn. (32), the following expression is obtained:

$$(2H_{VSC}/f^0)\frac{d}{dt}(\Delta f)=(NC_{DC}V_{DC}^0/S_{VSC})\frac{d}{dt}(\Delta V_{DC}) \quad (33)$$

Citation information: DOI 10.1109/TIE.2018.2835387, IEEE

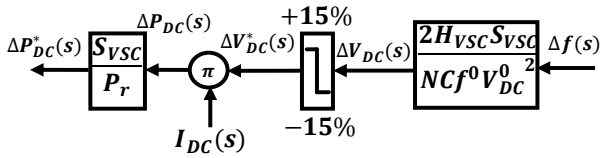

Fig. 5. Model of INEC Strategy for AGC Operation.

Taking Laplace transform on both sides:

$$(2H_{VSC}/f^0)s\Delta f(s) = (NC_{DC}V_{DC}^0/S_{VSC})s\Delta V_{DC}(s) \quad (34)$$

Or, $$\Delta V_{DC}(s) = (2H_{VSC}S_{VSC}/NC_{DC}f^0V_{DC}^0)\Delta f(s) \quad (35)$$

Dividing Eqn. (35) by V_{DC}^0 to convert DC voltage into per unit system, we get:

$$\Delta V_{DC}(s)\ (p.u.) = \left(\frac{2H_{VSC}\,S_{VSC}}{NC_{DC}\,f^0V_{DC}^{0\ 2}}\right)\Delta f(s) \quad (36)$$

The above equation directly relates the voltage deviations ΔV_{DC} of HVDC link with the frequency deviations Δf of AC system. Hence, it can be stated that in order to support the AC system from the stored energy of HVDC links for the duration of H_{VSC} seconds; HVDC link will be subjected to voltage deviations of ΔV_{DC} as per the Eqn. (36).

Practically, DC voltage fluctuations in HVDC links are allowed upto some extent. Therefore, DC voltage level must be restricted within upper and lower constraints. Typically, DC voltage of HVDC links are allowed to vary approximately in the range of ± 15 to $\pm 30\%$ of rated DC voltage. However, the exact values of upper and lower constraints depends upon the insulation level and current ratings of HVDC systems. The complete transfer function block diagram of proposed control for the utilization of stored energy from HVDC system is shown in Fig. 5. It can be observed that voltage deviation ΔV_{DC}^* has been multiplied by current I_{DC} to obtain the change in DC power output ΔP_{DC} in per unit. The value of I_{DC} is decided by the loading of HVDC link, for example, in case of 50% loaded line, value of I_{DC} will be 0.5 p.u. i.e. 50% of its rate current. The factor S_{VSC}/P_r has also been multiplied to ΔP_{DC} to convert the per unit value of power output from HVDC system base, S_{VSC} to power system area base P_r.

B. Calculation of Required Practical Size of DC Capacitance for Stored Energy Support:

Using the differential form of Eqn. (33) given as follows:

$$(2H_{VSC}/f^0)\frac{df}{dt} = (NC_{DC}V_{DC}/S_{VSC})\frac{dV_{DC}}{dt} \quad (37)$$

Integrating Eqn. (37) yields the following expression:

$$(2H_{VSC}/f^0)\int df = (NC_{DC}/S_{VSC})\int V_{DC}\,dV_{DC} \quad (38)$$

Or, $$(2H_{VSC}/f^0)f = (NC_{DC}V_{DC}^2/2S_{VSC}) + K \quad (39)$$

Where constant K is the integration coefficient which has been obtained as per the specified values of HVDC physical parameters, such as, inertia constant H_{VSC}, converter's power ratings S_{VSC}, rated DC voltage V_{DC}^0 and total system DC capacitance $N \times C_{DC}$. Substituting, $f = f^0$ and $V_{DC} = V_{DC}^0$ in Eqn. (39) to obtain 'K' for initial conditions, we get:

$$K = \frac{2H_{VSC}}{f^0}f^0 - \frac{NC_{DC}V_{DC}^{0\ 2}}{2S_{VSC}} \quad (40)$$

Putting back the value of 'K' in Eqn. (39) yields:

$$\frac{2H_{VSC}}{f^0}f = \frac{NC_{DC}V_{DC}^2}{2S_{VSC}} + \left(\frac{2H_{VSC}\,f^0}{f^0} - \frac{NCV_{DC}^{0\ 2}}{2S_{VSC}}\right) \quad (41)$$

Or, $$2H_{VSC}\left(\frac{f-f^0}{f^0}\right) = \frac{NC_{DC}}{2S_{VSC}}\left(V_{DC}^{\ 2} - V_{DC}^{0\ 2}\right) \quad (42)$$

Or, $$H_{VSC}\frac{\Delta f}{f^0} = \frac{NC_{DC}V_{DC}^{0\ 2}}{4S_{VSC}}\left[\left(\frac{V_{DC}}{V_{DC}^0}\right)^2 - 1\right] \quad (43)$$

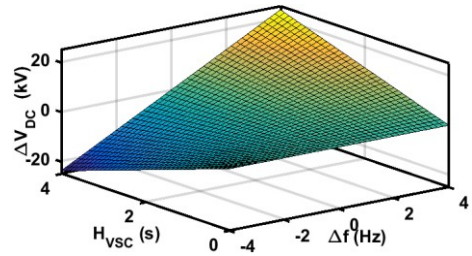

Fig. 6. Three dimensional view of relationship between ΔV_{DC}, Δf and H_{VSC}.

Substituting V_{DC}=$V_{DC}^0 + \Delta V_{DC}$ in Eqn. (43) yields the following expression:

$$H_{VSC}\frac{\Delta f}{f^0} = \frac{NC_{DC}V_{DC}^{0\ 2}}{4S_{VSC}}\left[\left(1 + \frac{\Delta V_{DC}}{V_{DC}^0}\right)^2 - 1\right] \quad (44)$$

Applying Taylor series expansion upon Eqn. (44):

$$H_{VSC} = \frac{NC_{DC}V_{DC}^{0\ 2}f^0}{4S_{VSC}\,\Delta f}\left[\left(1 + \frac{2\Delta V_{DC}}{V_{DC}^0}\right) - 1\right] \quad (45)$$

As we know that $V_{DC}^0 \gg \Delta V_{DC}$, thus the higher order terms of expansion series, such as, $\Delta V_{DC}^{\ 2}/V_{DC}^{0\ 2}$, $\Delta V_{DC}^{\ 3}/V_{DC}^{0\ 3}$…will become smaller and smaller. Therefore, these higher order terms have been neglected. This approximation yields the following expression:

$$H_{VSC} = \frac{NC_{DC}f^0V_{DC}^0\Delta V_{DC}}{2S_{VSC}\,\Delta f} \quad (46)$$

Using Eqn. (46), the required physical size of DC capacitance of HVDC link can be calculated for the desirable values of inertia constant H_{VSC}, maximum allowable limits of frequency change Δf, DC voltage deviations ΔV_{DC} and number of capacitors N present in the HVDC links. However, here it is important to note that the parameters of Eqn. (46) given as: N, f^0, V_{DC}^0, V_{DC}, S_{VSC} & Δf are fixed for a pre-defined HVDC system. Hence in this case, synthetic inertia of HVDC link becomes directly proportional to the required DC capacitor size i.e. $H_{VSC} \propto C_{DC}$. Now, we have to make a balance between these two parameters. Selecting the higher values of synthetic inertia will increase the required size of DC capacitance. Therefore, before selecting the value of synthetic inertia, we have to make sure that the required size of HVDC link capacitance is feasibly possible for the implementation of INEC strategy. For example, given values of parameters: $H_{VSC} = 4s$, $\Delta V_{DC} = 90$kV (30% of rated DC voltage V_{DC}=300kV), $\Delta f = 0.1Hz$, $N = 2$ (three-level neutral-point clamped VSC), S_{VSC}=600MW, the required size of HVDC capacitance as per the Eqn. (46) is given as: C_{DC}=0.148mF.

C. Some Practical Implementation Aspects of INEC Strategy for AGC Operations:

It has been proved that stored energy of HVDC links have the capability to support AC system during load disturbances in the form of inertia time constant H_{VSC} provided that HVDC voltage ΔV_{DC} is allowed to vary within the prescribed limits. Eqn. (46) shows the relationship between HVDC link parameters H_{VSC}, Δf and ΔV_{DC}. The following equation has been plotted in three-dimensional graph as shown in Fig. 6. The figure shows the variation in system DC voltage due to HVDC inertia time constant H_{VSC} varying in the range of 0−4s for the specified values of system frequency deviations Δf. Furthermore, it is also observed that the voltage deviation of HVDC link is inversely proportional to DC capacitance. This indicates that to avoid wide variations in DC voltage,

Citation information: DOI 10.1109/TIE.2018.2835387, IEEE

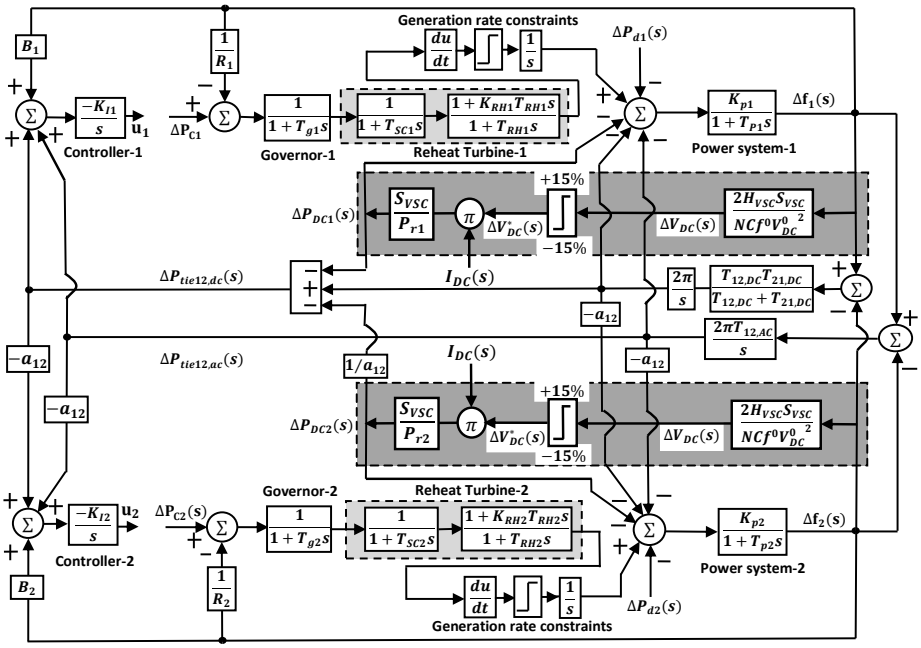

Fig. 7. Transfer function model of two-area reheat thermal power system with AC-DC interconnections.

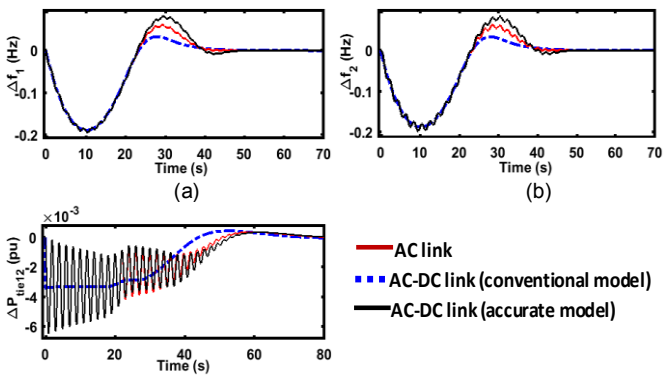

Fig. 8. Case I: GRCs are considered: (a) & (b) depict frequency deviation curves and (c) represents tie-line power deviation curves.

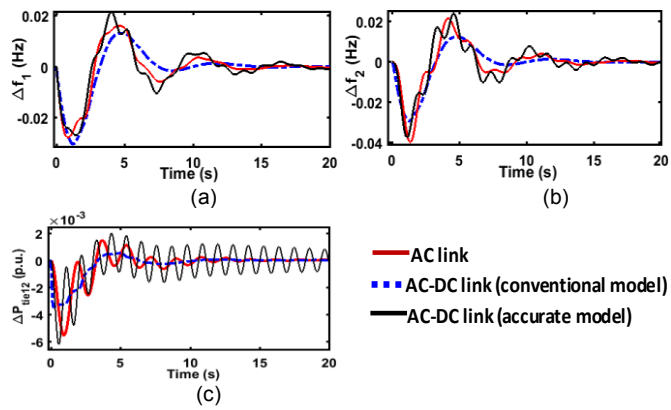

Fig. 9. Case II: GRCs are neglected: (a) & (b) depict frequency deviation curves and (c) represents tie-line power deviation curves.

large size DC capacitors must be used for HVDC links. The larger DC capacitors will require extra efforts for the protection of HVDC links. However, if the system DC voltage is allowed to vary upto some extent, then smaller DC capacitances can also be used.

V. System Investigated

Two unequal areas of reheat-thermal power system with AC-DC interconnections have been considered for investigations, as shown in Fig. 7 [1, 2]. The system parameter values are given in the Appendix II. The HVDC link has been modeled using proposed transfer function model. Furthermore, the proposed INEC strategy of HVDC links has also been incorporated in both power system areas of AGC. The energy absorbed/discharged by HVDC links must be supplied back to restore the system DC voltage. Therefore, energy supplied by HVDC links has been subtracted from the HVDC tie-line power which implies that a portion of HVDC tie-line power has been supplied to restore the DC link voltage while the other portion goes to respective power system areas for secondary/supplementary control. The controller gains have been tuned using integral squared error (ISE) criterion. The performance index 'J' of ISE criterion is given as follows:

$$J = \sum_{k=1}^{n} \left\{ |\Delta f_i(k)|^2 + \left|\Delta P_{tieij}(k)\right|^2 \right\} \Delta T \qquad (47)$$

The particle swarm optimization (PSO) has been used for the minimization of performance index 'J' [8, 11].

VI. Simulation Results and Discussions

The study has been divided into two parts. In the first part, conventional model of HVDC link has been compared with the accurate model, while in second part, proposed INEC strategy to harness the stored energy of HVDC links for AGC operation has been evaluated. These studies are as follows:

A. Conventional vs. Accurate Model of HVDC Tie-Links:

The dynamic performance of AGC system based on conventional and accurate model of HVDC links has been compared. The data of DC and AC links have been shown in Tables I & II, respectively. The two case studies are performed given as follows:

Citation information: DOI 10.1109/TIE.2018.2835387, IEEE

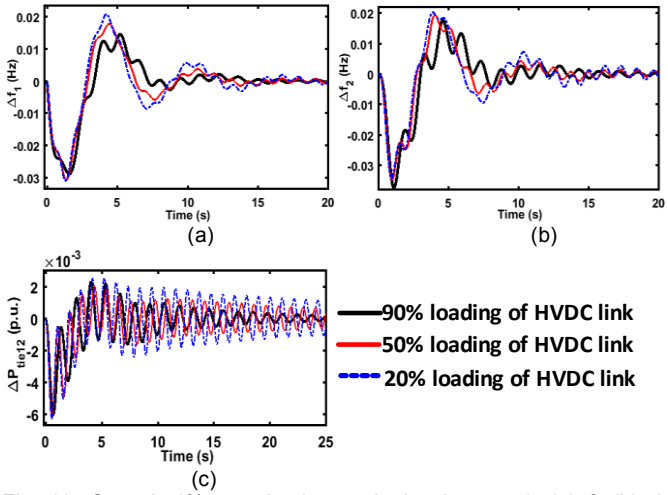

Fig. 10. Case I: 1% step load perturbation in area-1: (a) & (b) depict frequency deviation curves, (c) represents tie-line power deviation curves.

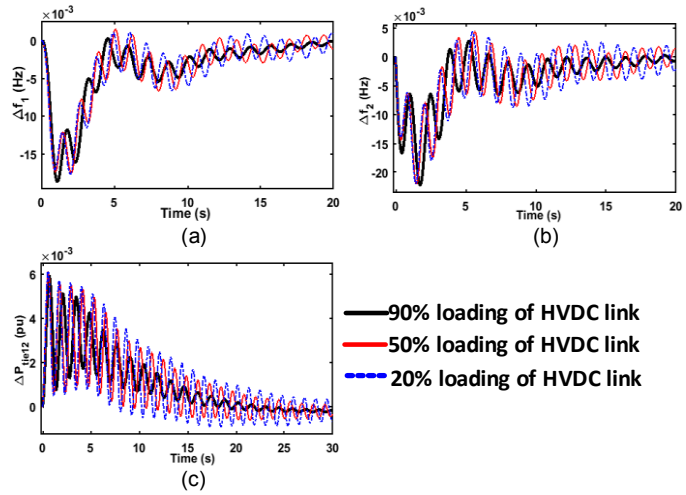

Fig. 11. Case II: 1% step load perturbation in area-2: (a) & (b) depict frequency deviation curves and (c) shows tie-line power deviation curves.

1) Study of AGC dynamic performance at the fixed loading conditions of HVDC links

Both AC and DC links are loaded equally upto 50% of their rated capacities. The synchronizing coefficients of AC and DC links for 50% loading condition are 0.0865 and 0.129, respectively. The step load perturbation of 1% magnitude has been given in area-1. The optimized values of controller gains are given in Appendix II. The system dynamic responses have been obtained for two cases. In this first case, system GRCs of 3% per minute have been considered to restrict the thermal generating unit's power outputs; while in the second case, system GRCs have been neglected. The dynamic responses for these two cases are shown in Figs. 8 & 9, respectively. In these figures, dynamic responses have been compared obtained for the systems having AC link, AC-DC link with conventional model and AC-DC link with accurate model of HVDC link. It has been observed that the conventional model of HVDC link depicts the improvement in system dynamic performance irrespective of considering system GRCs, when it is added in parallel to AC link. However, the proposed accurate model of HVDC tie-line just shows the opposite trend i.e. the addition of HVDC link in parallel to the existing AC link do not improve the AGC dynamic performance, instead the system becomes more oscillatory in nature for both cases, with and without system GRCs. The main reason behind the degradation in system dynamic performance is that the HVDC tie-link exhibits its own synchronization coefficient. Therefore, adding it in parallel to AC link increases the overall synchronization coefficient of entire AC-DC link.

2) Study of AGC dynamic performance at different loading conditions of HVDC links

The investigations are also carried out to study the AGC dynamic performance at different loading conditions of HVDC links. The values of synchronization coefficients (T_{eqv}) of HVDC link for 90%, 50% and 20% loading conditions are given in Table III. It has been observed from the table that as the loading of HVDC link varies from 90% to 20%, synchronization coefficient of HVDC link also varies from 0.0654 to 0.146. The system dynamic responses have been obtained for different values of synchronization coefficients acquired from different loading conditions of HVDC link. Here, two cases are studied. In first case, 1% step load perturbation (SLP) has been considered in area-1, while in the second case, 1% SLP has been considered in area-2. The system dynamic responses for these two cases are shown in Figs. 10 and 11, respectively. The system dynamic responses shows that as the loading of HVDC link decreases or in other words, as the value of HVDC synchronization coefficient increases, system dynamic performance deteriorates in terms of number of oscillations and settling time irrespective to the location of power system load disturbances. Hence, it can be concluded that the proposed accurate transfer function model of HVDC link demonstrates the dependency of its model parameters upon the loading of tie-link and affects the system dynamic performance similar to the AC links.

B. Evaluation of Proposed INEC Strategy for AGC Operation:

The proposed INEC strategy to utilize the stored energy of HVDC links in AGC operation has been evaluated under two case studies. In the first case study, proposed control strategy has been evaluated under step load as well as continuous power system load disturbances. In the second case study, proposed control strategy has been evaluated for different values of HVDC link model parameters. These case studies are as follows:

1) Evaluation of INEC Strategy under Step Load Disturbances of Power System

The proposed control strategy for AC-DC interconnected system has been compared with the normal AC-DC system. The system dynamic responses have been obtained for step load perturbations in area-1, as shown in Figs. 12(a)–(e). In these figures, various AGC system output responses, such as, frequency deviations, tie-line power deviations and voltage deviations in HVDC link have been shown for comparative analysis. These dynamic responses clearly shows that the proposed control strategy demonstrate the better dynamic performance in terms of maximum undershoot, subsequent oscillations and settling time. The voltage deviation curve of

Citation information: DOI 10.1109/TIE.2018.2835387, IEEE

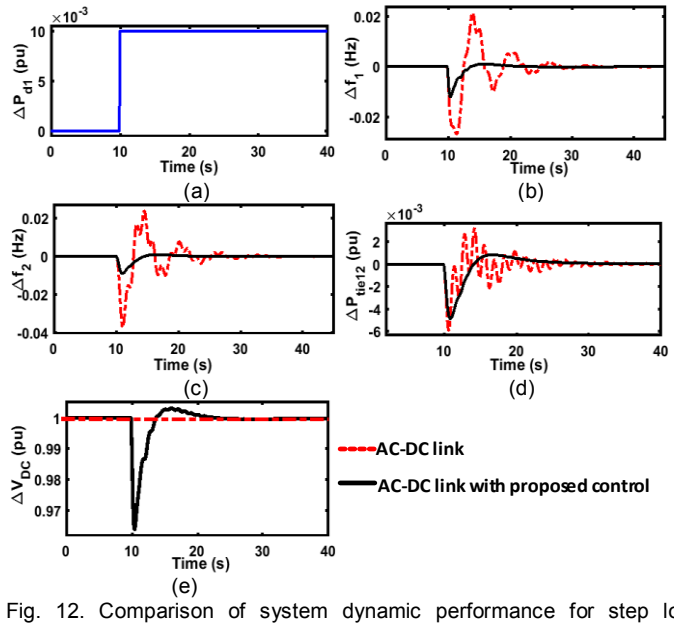

Fig. 12. Comparison of system dynamic performance for step load disturbances of power system: (a) is load disturbance in area-1, (b) & (c) are frequency deviations, (d) is tie-line power deviation and (e) is voltage deviation of HVDC link.

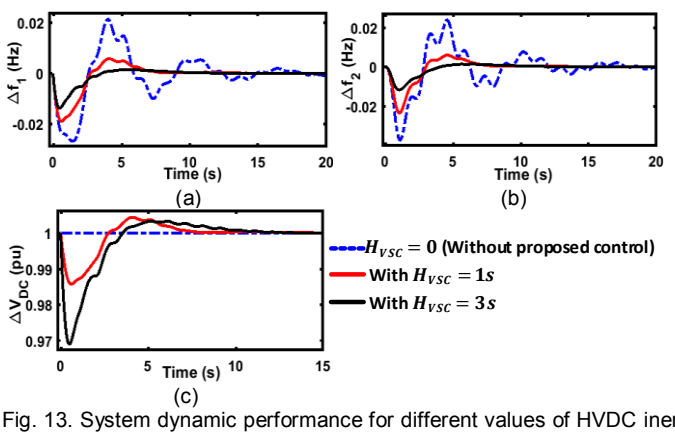

Fig. 13. System dynamic performance for different values of HVDC inertia constants H_{VSC}: (a) &(b) are the frequency deviation curves and (c) is the change in voltage deviations of HVDC link.

HVDC tie-link has also been shown in Figs. 12(e). It has been observed that in case of proposed control strategy, DC voltage level of HVDC link fluctuates considerably due to the utilization of stored energy of HVDC system. However, this voltage deviation diminishes quickly as the discharged energy of HVDC tie-link restores back to its nominal condition.

2) Evaluation for INEC Strategy for Different Values of HVDC Link Model Parameters

The proposed control strategy for AC-DC interconnected system has been evaluated under different values of HVDC link model parameters, namely, inertia constant (H_{VSC}) and dc capacitance (C_{DC}). The system dynamic responses obtained for different values of H_{VSC} varying in the range of 0 to 3s are shown in Fig. 13. It has been observed that as the value of H_{VSC} increases, the system dynamic performance improves. It can be clearly observed from Figs. 13(a) & (b), that the maximum peaks, subsequent and settling time of frequency deviation curves have been reduced considerably with the increased values H_{VSC}. However, at the same time fluctuations

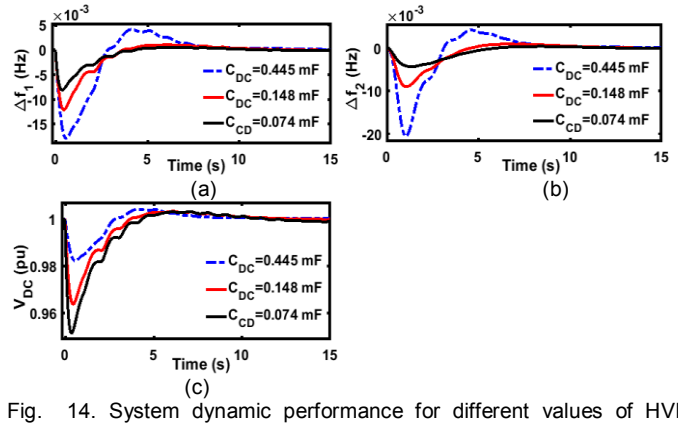

Fig. 14. System dynamic performance for different values of HVDC capacitance C_{DC} where (a) & (b) are the frequency deviations and (c) represents the change in voltage level of HVDC link.

TABLE IV EIGEN VALUES FOR DIFFERENT VALUES OF HVDC LINK MODEL PARAMETERS

Modes	$T_{eqv} = 0.0867$	$T_{eqv} = 0.1732$	$T_{eqv} = 0.1954$
$\boldsymbol{\lambda_1}$	$\mathbf{-33.47+ i0}$	$\mathbf{-30.47+ i0}$	$\mathbf{-28.47+ i0}$
λ_2	$-33.46+ i0$	$-33.46+ i0$	$-33.46+ i0$
$\boldsymbol{\lambda_3}$	$\mathbf{-0.751+ i4.88}$	$\mathbf{-0.754+ i5.83}$	$\mathbf{-0.755+ i6.055}$
$\boldsymbol{\lambda_4}$	$\mathbf{-0.751- i4.88}$	$\mathbf{-0.754- i5.83}$	$\mathbf{-0.755- i6.055}$
λ_5	$-3.014- i0$	$-3.169- i0$	$-3.197- i0$
$\boldsymbol{\lambda_6}$	$\mathbf{-1.79+ i1.57}$	$\mathbf{-1.00+ i1.90}$	$\mathbf{-0.69+ i2.01}$
$\boldsymbol{\lambda_7}$	$\mathbf{-1.79- i1.57}$	$\mathbf{-1.00- i1.90}$	$\mathbf{-0.69- i2.01}$
λ_8	$-0.744+ i0$	$-0.742+ i0$	$-0.731+ i0$
λ_9	$-0.401+ i0$	$-0.400+ i0$	$-0.380+ i0$
λ_{10}	$-0.219+ i0$	$-0.219+ i0$	$-0.219+ i0$
λ_{11}	$-0.199+ i0$	$-0.199+ i0$	$-0.199+ i0$

in voltage level of HVDC tie-link (V_{DC}) have been increased, as shown in Fig. 14(c).

The system dynamic responses have also been obtained for different values of DC capacitance as shown in Figs. 14(a) & (b). It has been observed that selecting higher value of DC capacitance degrades the system dynamic performance. However, at the same time fluctuations in HVDC link voltage also decreases as shown in Fig. 14(c). Hence, it can be concluded that selecting higher value of DC capacitance reduces fluctuations in DC voltage. However, allowing the DC voltage fluctuations upon to some pre-specified limits will not only reduce the requirement of large size DC capacitors, but also improve the AGC dynamic performance.

C. Eigen Value Analysis of Proposed HVDC Link Model:

The Eigen value analysis has been performed to study the impact of HVDC link model parameters on AGC dynamic performance. In order to perform state space analysis, AGC system has been represented by following state space model given as:

$$\dot{\bar{x}} = A\bar{x} + B\bar{u} + F\bar{w} \tag{48}$$

$$\bar{y} = C\bar{x} \tag{49}$$

Where, $\bar{x}$ =State matrix, $\bar{u}$ = Control vector, $\bar{w}$ = Disturbance vector, A =State distribution matrix, B =Control distribution matrix, C =Output matrix and F =Disturbance matrix. The 11 state variables have been considered for state space analysis given as follows:

$x_1 = \Delta f_1$, $x_2 = \Delta P_{g1}$, $x_3 = \Delta P_{r1}$, $x_4 = \Delta X_{g1}$, $x_5 = \Delta P_{tie} = \Delta P_{tie\,12,dc} + \Delta P_{tie\,12,ac}$, $x_6 = \int ACE_1$, $x_7 = \Delta f_2$, $x_8 = \Delta P_{g2}$, $x_9 = \Delta P_{r2}$, $x_{10} = \Delta X_{g2}$, $x_{11} = \int ACE_2$

Citation information: DOI 10.1109/TIE.2018.2835387, IEEE

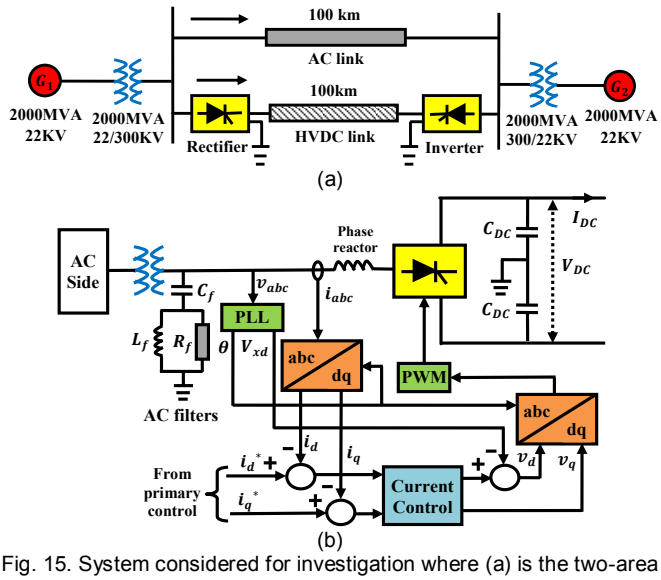

Fig. 15. System considered for investigation where (a) is the two-area power system with AC-HVDC link and (b) is the control system used to control VSC−HVDC links.

The matrices A, B, C and F obtained from the state space model have been given in the Appendix III. Finding control vector $\bar{u}$ which minimizes the performance index is given as:

$$J = \frac{1}{2}\int_0^{\infty}(\bar{x}^T Q\bar{x} + \bar{u}^T R\bar{u})\, dt \qquad (50)$$

The above equation has been solved using Riccati equation [28]. The Eigen values obtained for different values of proposed HVDC link model parameters have been shown in Table IV. The HVDC link model parameter T_{eqv} has been varied from 0.0867 to 0.1954 and corresponding Eigen values have been obtained. It has been observed that as the value of HVDC link synchronization coefficient increases, modes λ_1, λ_6 and λ_7 moves towards right side of complex s-plain, while the imaginary part of modes λ_3 and λ_4 increases in size. This indicates that system dynamic performance deteriorates in terms of undershoots and oscillations with increased value of HVDC link synchronization coefficient.

D. Validation of Proposed Model of HVDC Link:

The detailed physical simulation study has been performed using '*Simpower System/Matlab*' software platform in order to validate the proposed model of HVDC links. The system considered for simulation study has been shown in Fig. 15(a). The *'vector control'* method has been used to regulate the tie-line power of HVDC link as shown in Fig. 15(b). The 100kms transmission lines are selected for both AC as well as HVDC links. The details of physical components and parameter values are given in Appendix IV. The validation has been performed into three different comparative case studies given as follows:

1) In the first case, conventional first-order transfer function model of HVDC link has been tested with the physical simulation study of AGC system. The simulation results have been obtained for AC-DC link with the conventional and simpower models as shown in Fig. 16. Both, AC and HVDC links has been considered to be loaded at 50% of their rated capacities. These simulation results complements the findings of proposed HVDC link model is that adding HVDC links in parallel to AC link degrades AGC dynamic performance.

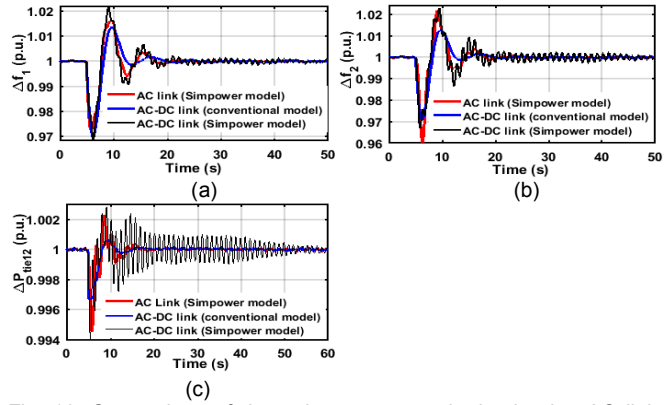

Fig. 16. Comparison of dynamic responses obtained using AC link, AC-DC with conventional model, AC-DC link with simpower model.

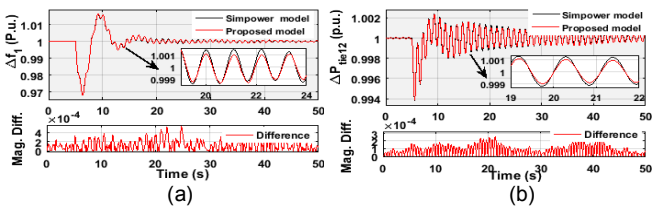

Fig. 17. Comparison of system dynamic responses obtained using proposed model and simpower model of HVDC links.

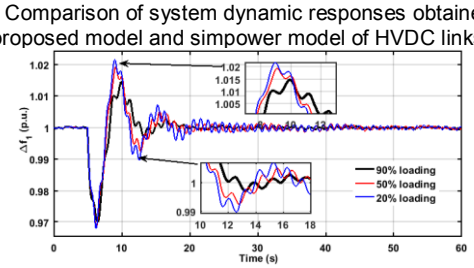

Fig. 18. System frequency deviation at different loading conditions of HVDC link obtained using Matlab/simpower software platform.

2) In the second case, the accuracy of proposed HVDC link model has been tested with physical simulation study of AGC system. The system dynamic responses using proposed and simpower models of HVDC link have been shown in Fig 17. It has been observed that the maximum magnitude of error between these models varies in the range of 3 to 4×10^{-4}, which is considerably small and can be neglected. The reason of this error is due to the fact that physical simulation study involves non-linear dynamics of generators and other components of power systems participating in AGC operations.

3) In the third case, system dynamic responses have also been obtained for different loading conditions of HVDC link using physical simulation of AGC system. These system dynamic responses have been shown in Fig. 18. It has been observed that system dynamic performance deteriorates as the HVDC link loading decreases from its rated/nominal loading condition. Hence, all these physical simulation studies complement the findings of proposed model of HVDC link.

Here, it is important to note that when HVDC tie-line power again converted into AC power, it needs to be first synchronized with the other interconnected power system area. Typically, phase locked loops (PLLs) are used for this purpose. The quality/degree of synchronization between power system areas affects AGC dynamic performance.

Citation information: DOI 10.1109/TIE.2018.2835387, IEEE

Hence, synchronizing coefficient of HVDC link plays a significant role in power system dynamics. In previous AGC studies, aforementioned synchronization aspect of HVDC link was completely ignored in existing transfer function model of HVDC link. The existing model is independent of this HVDC link's synchronization characteristic. However, proposed model incorporates the synchronization characteristic and describes its detailed dynamic behavior against the interconnected grid. It shows that AGC dynamic performance depends upon the synchronization coefficient or in other words depends upon the degree of synchronization similar to AC link. The loading of HVDC links changes the degree of synchronization between interconnecting power system areas. As a result, it also changes the value of synchronization coefficient and in turn it affects the AGC dynamic performance. Finally based on the aforementioned findings, it can be concluded that it was system design issue which was not taken into account in previous AGC studies.

VII. Conclusions

The significant contributions are given as follows:

1) For the first time, transfer function model of HVDC links has been derived mathematically with physical as well as analytical justifications. The model shows that adding HVDC link in parallel to AC link do not always improves the AGC dynamic performance; instead system dynamic performance depends upon the loading of HVDC link. As the loading of HVDC link decreases, system dynamic performance deteriorates due to the increased value of HVDC link synchronizing coefficient. The inferences drawn remain the same for both cases, with and without system GRCs. The detailed simulation studies have also been performed in order to validate the proposed model of HVDC links.

2) Furthermore proposed accurate model of HVDC link also reveals that the HVDC links have their own synchronization coefficients similar to AC links. The power transfer between the interconnecting power system areas via HVDC links depends upon these synchronization coefficients.

3) It has also been proved analytically that the synchronization coefficient of HVDC link is just half to that of AC link for equal power transfer capability and loadings of both tie-links. This indicates that if an AC link is completely replaced by HVDC link of same size and capacity, then the HVDC link will always exhibit better dynamic performance in comparison to AC link because of its lesser value of torque synchronization coefficient. However, if the HVDC link is being added in parallel to AC link, then the system dynamic performance depends upon the overall synchronization coefficient of AC-DC link. The study shows that HVDC link synchronization coefficient decreases as the tie-link loading reaches to its rated condition. Therefore, it is recommended to operate HVDC links near to their ratings in order to achieve better system dynamic performance.

4) The INEC strategy has been implemented in AGC to utilize the stored energy of HVDC links for AGC operation. Alongside physical and analytical justifications, the proposed control strategy has been successfully implemented upon two-area reheat thermal power system. To demonstrate the superiority of proposed control strategy, AGC system has been tested for step load disturbances of power system. In each and every case, proposed control strategy demonstrates better dynamic performance in terms of maximum undershoot, subsequent oscillations and settling time.

5) The INEC strategy allows to varying the HVDC link voltage upto some pre-specified limits. Therefore, the impact of various system parameters, mainly inertia constant H_{VSC} and capacitance C_{DC} on HVDC system voltage has also been studied. It has been discovered that selecting the higher values of H_{VSC} and the lower values C_{DC} improves the system dynamic performance. However, at the same time fluctuations in HVDC system voltage also increases. Therefore, selecting the values of H_{VSC} and C_{DC} is the most critical part of the proposed control strategy. These values of H_{VSC} and C_{DC} must be selected after keeping in view the maximum allowable limits of HVDC system voltage variations.

Appendix I

(a) AC link: The synchronization coefficient for AC link as shown in Fig. 1(b), can be written as follows:

$$T_{12,AC} = P_{max,AC}\cos(\delta_1^0 - \delta_2^0) \tag{48}$$

Where: $P_{max,AC} = (V_1V_2/X_L)$ represents the maximum power transfer capacity of AC link.

(b) DC link: The synchronization coefficient has been derived for HVDC link is given as follows:

$$T_{eqv,DC} = T_{12,DC}T_{21,DC}/\left(T_{12,DC} + T_{21,DC}\right) \tag{49}$$

Where:

$$T_{12,DC} = P_{max,DC}\cos(\delta_1^0 - \gamma_1^0)\ \&\ T_{21,DC} = P_{max,DC}\cos(\delta_2^0 - \gamma_2^0) \tag{50}$$

It is assumed that maximum power transfer capabilities of both AC and DC links are equal i.e. $P_{max,AC} = P_{max,DC}$. Further, both links are equally loaded. Hence, bus angle differences for both tie-links must be equal i.e. $\delta_1^0 - \delta_2^0 = \delta_1^0 - \gamma_1^0 = \delta_2^0 - \gamma_2^0$ (for example, at 50% loading condition, all the bus angle differences will be 30^0).

Applying these assumptions in Eqns. (48) & (50), following expression is obtained:

$$T_{12,AC} = T_{12,DC} = T_{21,DC} \tag{51}$$

Substituting Eqn. (51) into Eqn. (49), the following relation is obtained:

$$T_{eqv,DC} = T_{12,AC}/2 \tag{52}$$

Appendix II

- *Parameters values of two-area reheat thermal power system:*

f^0=60Hz, P_{r1}=2000MW, P_{r2}=1000MW, $T_{p1} = T_{p2}$=20s, $T_{SC1} = T_{SC2}$=0.3s, $K_{RH1} = K_{RH2}$ =0.5, R_1=R_2=2.4Hz/$MW_{p.u.}$, K_{p1}=K_{p2}=120.048Hz/$MW_{p.u.}$, B_1=B_2= 0.425$MW_{p.u.}$/Hz, T_{g1}=T_{g2}=0.08s and a_{12}=2.

- *Optimized values of supplementary controller gains:*

(a) With GRCs: K_{I1}=0.255, K_{I2}=0.151 *(b)* Without GRCs: K_{I1}= 0.686, K_{I2}= 0.117

Appendix III

$A = [A_{11} \quad A_{12}]$, where matrices A_{11} and A_{12} are given as follows:

$$A_{11} = \begin{bmatrix} -\frac{1}{T_{p1}} & \frac{K_{p1}}{T_{p1}} & 0 & 0 & -\frac{K_{p1}}{T_{p1}} & 0 \\ 0 & -\frac{1}{T_{RH1}} & \left(\frac{1}{T_{RH1}} - \frac{K_{RH1}}{T_{SC1}}\right) & \frac{K_{RH1}}{T_{SC1}} & 0 & 0 \\ 0 & 0 & -\frac{1}{T_{SC1}} & \frac{1}{T_{SC1}} & 0 & 0 \\ -\frac{1}{R_1T_{g1}} & 0 & 0 & -\frac{1}{T_{g1}} & 0 & 0 \\ 2\pi\left(T_{eqv} + T_{12,AC}\right) & 0 & 0 & 0 & 0 & 0 \\ B_1 & 0 & 0 & 0 & 1 & 0 \\ 0 & 0 & 0 & 0 & \frac{a_{12}K_{p2}}{T_{p2}} & 0 \\ 0 & 0 & 0 & 0 & 0 & 0 \\ 0 & 0 & 0 & 0 & 0 & 0 \\ 0 & 0 & 0 & 0 & 0 & 0 \\ 0 & 0 & 0 & 0 & -a_{12} & 0 \end{bmatrix}_{11\times 6}$$

Citation information: DOI 10.1109/TIE.2018.2835387, IEEE

$$A_{11}=\begin{bmatrix} 0 & 0 & 0 & 0 & 0 \\ 0 & 0 & 0 & 0 & 0 \\ 0 & 0 & 0 & 0 & 0 \\ 0 & 0 & 0 & 0 & 0 \\ -2\pi\left(T_{eqv}+T_{12,AC}\right) & 0 & 0 & 0 & 0 \\ 0 & 0 & 0 & 0 & 0 \\ -\frac{1}{T_{p2}} & \frac{K_{p2}}{T_{p2}} & 0 & 0 & 0 \\ 0 & -\frac{1}{T_{RH2}} & \left(\frac{1}{T_{RH2}}-\frac{K_{RH2}}{T_{SC2}}\right) & \frac{K_{RH2}}{T_{SC2}} & 0 \\ 0 & 0 & -\frac{1}{T_{SC2}} & \frac{1}{T_{SC2}} & 0 \\ -\frac{1}{R_2T_{g2}} & 0 & 0 & -\frac{1}{T_{g2}} & 0 \\ B_2 & 0 & 0 & 0 & 0 \end{bmatrix}_{11\times 5}$$

$$B=\begin{bmatrix} 0 & 0 & 0 & \frac{1}{T_{g1}} & 0 & 0 & 0 & 0 & 0 & 0 & 0 \\ 0 & 0 & 0 & 0 & 0 & 0 & 0 & 0 & 0 & \frac{1}{T_{g2}} & 0 \end{bmatrix}^T$$

$$F=\begin{bmatrix} -\frac{K_{p1}}{T_{p1}} & 0 & 0 & 0 & 0 & 0 & 0 & 0 & 0 & 0 & 0 \\ 0 & 0 & 0 & 0 & 0 & 0 & -\frac{K_{p1}}{T_{p1}} & 0 & 0 & 0 & 0 \end{bmatrix}^T$$

APPENDIX IV

Components	Details
Converters type	3-level bridge (IGBT) type
Converter control	Vector control
HVDC line model	π −model
AC line model	Distributed line model
Numerical solver	Discrete ode23tb(stiff/TR-BDF2)
Solver step size	6.173μsec

- *Generator parameters:* Stator resistance (r_s)=0.0045p.u., rotor type=salient pole, rpm=3600, d-axis reactances (p.u.) X_d=1.305, X'_d =0.296, X''_d =0.252, q-axis reactances (p.u.) X_q=0.474, X''_q =0.243, leakage reactance (p.u.) X_l =0.18.
- *Speed governor control valve parameters:* V_{gmin} = −0.1p.u./s, V_{gmax} =0.1p.u./s, V_{min} =0, V_{max} =4.496p.u.
- *Transformer parameters:* r =7.8× 10^{-4}, L =0.15p.u., r_m =500p.u., L_m =500p.u.

REFERENCES

[1] X. Su, X. Liu, Y.D. Song, "Event-Triggered Sliding-Mode Control for Multi-Area Power Systems," *IEEE Trans. on Industrial Electronics*, vol. 64, no. 8, pp. 6732-6741, 2017.

[2] M. Ma, C. Zhang, X. Liu, "Distributed Model Predictive Load Frequency Control of the Multi-Area Power System After Deregulation," *IEEE Trans. on Industrial Electronics*, vol. 64, no. 6, pp. 5129-5139, 2017.

[3] V.P. Singh, N. Kishor, P. Samuel, "Distributed Multi-Agent System-Based Load Frequency Control for Multi-Area Power System in Smart Grid," *IEEE Trans. on Industrial Electronics*, vol. 64, no. 6, pp. 5151-5160, 2017.

[4] X. Liu, Y. Zhang, K.Y. Lee, "Coordinated Distributed MPC for Load Frequency Control of Power System With Wind Farms," *IEEE Trans. on Industrial Electronics*, vol. 64, no. 4, pp. 5140-5150, 2017.

[5] J.J. Ibarra, M.I. Morales, W.J. Cabrera *et al.*, "AGC Parameter Determination for an Oil Facility Electric System," *IEEE Trans. on Industry Applications*, vol. 50, no. 4, pp. 2876-2882, 2014.

[6] S.K. Aditya, D. Das, "Design of Load Frequency Controllers Using Genetic Algorithm for Two Area Interconnected Hydro Power System," *Elect. Power Compt. Syst.*, vol. 31, no. 1, pp. 81−94, 2003.

[7] C.K. Shiva, V. Mukherjee, "Automatic generation control of multi-unit multi-area deregulated power system using a novel quasi-oppositional harmony search algorithm," *IET Generation, Transmission & Distribution*, vol. 9, no. 15, pp. 2398–2408, 2015.

[8] C. Mu, Y. Tang, H. HeImproved, "Improved Sliding Mode Design for Load Frequency Control of Power System Integrated an Adaptive Learning Strategy," *IEEE Trans. on Industrial Electronics*, vol. 64, no. 8, pp. 6742-6751, 2017.

[9] N. Pathak, T.S. Bhatti, A. Verma, "Discrete Data AGC of Hydro-Thermal Systems under Varying Turbine Time Constants along with the Power System loading Conditions," *IEEE Trans. on Industry Applications*, vol. PP, 99, pp. 1-13, 2017. (Early access article)

[10] N. Pathak, T.S. Bhatti, A. Verma, "Accurate Modelling of Discrete AGC Controllers for interconnected Power Systems," *IET Generation, Transmission & Distribution*, vol. 11, no. 6, pp. 2102-2114, 2017.

[11] G. Sharma, I. Nasiruddin, K.R. Niazi *et. al.*, "Robust automatic generation control regulators for a two-area power system interconnected via AC/DC tie-lines considering new structures of matrix Q," *IET Generation, Transmission & Distribution*, vol. 10, no. 14, pp. 3570−3579, 2016.

[12] Y. Arya, N. Kumar, "AGC of a multi-area multi-source hydrothermal power system interconnected via AC/DC parallel links under deregulated environment," *Int. J. Electr. Power Energy Syst.*, vol. 75, pp. 127−138, 2016.

[13] N.J.V. Kumar, M.M.T. Ansari, "A new design of dual mode Type-II fuzzy logic load frequency controller for interconnected power systems with parallel AC–DC tie-lines and capacitor energy storage unit," *Int. J. Electr. Power Energy Syst.*, vol. 82, pp. 579−598, 2016.

[14] N.J.V. Kumar, M.M.T. Ansari, "A new design of dual-mode Type-II fuzzy logic load frequency controller for interconnected power systems with parallel AC-DC tie-lines and superconducting magnetic energy storage unit," *Energy*, vol. 89, pp. 118−137, 2015.

[15] S. Selvakumarana, S. Parthasarathy, R. Karthigaivel, *et. al.*, "Optimal Decentralized Load Frequency Control in a Parallel AC-DC Interconnected Power System Through HVDC Link Using PSO Algorithm," *Energy Procedia*, vol. 14, pp. 1849−1854, 2012.

[16] E. Rakhshani, K. Rouzbehi, M.A. Elsaharty, "Heuristic Optimization of Supplementary Controller for VSC-HVDC/AC Interconnected Grids Considering PLL," *Electric Power Components & Systems*, vol.45, no. 3, pp. 288−301, 2017.

[17] G. Sharma, I. Nasiruddin, K.R. Niazi, "Optimal Automatic Generation Control of Asynchronous Power Systems Using Output Feedback Control Strategy with Dynamic Participation of Wind Turbines," *Electric Power Components & Systems*, vol. 43, no. 4, pp. 384−398, 2015.

[18] J. Zhu, C.D. Booth, G.P. Adam, *et. al.*, "Inertia Emulation Control Strategy for VSC-HVDC Transmission Systems," *IEEE Trans. on Power Systems*, vol. 28, no. 2, pp. 1277-1287, 2013.

[19] A.J. Ferré, Y. Pipelzadeh, T.C. Green, "Blending HVDC-Link Energy Storage and Offshore Wind Turbine Inertia for Fast Frequency Response," *IEEE Trans. on Sustainable Energy*, vol. 6, no. 3, pp. 1059-1066, 2015.

[20] C. Du, E. Agneholm, G. Olsson, "Comparison of Different Frequency Controllers for a VSC-HVDC Supplied System," *IEEE Trans. on Power Delivery*, vol. 23, no. 4, pp. 2224-2232, 2008.

[21] J. Zhu, J.M. Guerrero, W. Hung, "Generic inertia emulation controller for multi-terminal voltage-source-converter high voltage direct current systems," *IET Renewable Power Generation*, vol. 8, no. 7, pp. 740-748, 2014.

[22] O.D. Adeuyi, M. Cheah-Mane, J. Liang, *et al.*, "Frequency support from modular multilevel converter based multi-terminal HVDC schemes," *Power & Energy Society General Meeting, 2015 IEEE*, pp. 1-5, 2015.

[23] A.S. Elansari, S.J. Finney, J. Burr, *et. al.*, "Frequency control capability of VSC-HVDC transmission system," *11th IET International Conference on AC and DC Power Transmission*, pp. 1-6, 2015.

[24] E. Rakhshani, P. Rodriguez, "Inertia Emulation in AC/DC Interconnected Power Systems Using Derivative Technique Considering Frequency Measurement Effects," *IEEE Trans. on Power Systems*, vol. 32, no. 5, pp. 3338-3351, 2017.

[25] X. Zhu, J. Cai, Q. Yan, *et. al.*, "Virtual inertia control of wind-battery-based islanded dc micro-grid," *International Conference on Renewable Power Generation (RPG 2015)*, pp. 1-6, 17-18 Oct, 2015.

[26] Cuiqing Du, "The control of VSC-HVDC and its use for large industrial power systems," *Ph.D. dissertation*, Department of Electric Power Engineering, Chalmers University of Technology, Goteborg, Sweden, 2003. (http://publications.lib.chalmers.se/records/fulltext/11875.pdf)

[27] H.F. Latorre, M. Ghandhari, L. Soder, "Multichoice Control Strategy for VSC-HVdc," *Bulk Power System Dynamics and Control-VII. Revitalizing Operational Reliability, 2007 iREP Symposium*, pp. 1-7, 19-24 Aug, 2007, South Carolina, USA.

[28] N. Pathak, I. Nasiruddin, T.S. Bhatti, "A More Realistic Model Of Centralized Automatic Generation Control In Real-Time Environment," *Electr. Power Comp. Systs.*, vol. 43, no. 29, pp. 2205-2213, 2015.

Citation information: DOI 10.1109/TIE.2018.2835387, IEEE

BIOGRAPHIES

Nikhil Pathak (S'17) received the B.Tech degree in electrical and electronics engineering from IIMT engineering College, Meerut, India, in 2012 and the M.Tech degree in electrical power system & management from Jamia Millia Islamia University, New Delhi, India, in 2014. He is currently working toward the Ph.D. degree in power system operation and control from the Centre for Energy Studies, Indian Institute of Technology Delhi, New Delhi, India. His research interest focuses on automatic generation control (AGC) of thermal and hydropower system as well as intelligent control techniques in AGC.

Ashu Verma (M'12–SM'17) received the M.Tech degree in power systems in 2002 and the Ph.D. degree in transmission expansion planning in 2010, both from Indian Institute of Technology Delhi, New Delhi, India. She is currently an Assistant Professor with the Centre for Energy Studies, Indian Institute of Technology, New Delhi. She also worked as an Assistant Engineer in Nathpa Jhakri Hydro Electric Project, H.P. Her current research interests include power system planning, operation and control aspects of integrated renewable energy systems, policy and regulatory framework for enabling large scale integration of renewable energy sources in India.

T.S. Bhatti received the Ph.D. degree in power system operation and control from the Department of Electrical Engineering, Indian Institute of Technology Delhi, New Delhi, India, in 1985. He is currently a Professor with the Centre for Energy Studies, Indian Institute of Technology Delhi. He has been involved in teaching and research at Indian Institute of Technology Delhi since 1980. During 1987, he was a Postdoctoral Fellow at the University of Newcastle, Callaghan, NSW, Australia. His research interests include reactive power control, automatic generation control, wind energy conversion systems and small-hydropower systems.

Ibraheem Nasiruddin received the Ph.D. degree in power systems from the Department of Electrical Engineering, Aligarh Muslim University (AMU), Aligarh, India, in 2000. He is currently working in the Department of Electrical Engineering, Qassim Engineering College, Qassim University, Kingdom of Saudi Arabia, as a Full Professor. Before taking this assignment, he worked at Jamia Millia Islamia, New Delhi, India, for more than 25 years as teaching faculty and in various other positions. His research interests include power system operation and control, optimal control theory applications in power systems, application of intelligent controls in deregulated power systems and renewable energy systems.